

Hierarchical Porous Nitrogen-Doped Spray-Dried Graphene for High Performance Capacitive Deionization

Owen Noonan, Yueqi Kong, Yang Liu, Mohammed Kalantari, Ashok Kumar Nanjundan, Xiaodan Huang, and Chengzhong Yu*

Graphene foam materials have attracted particular attention for capacitive deionization (CDI) applications due to their robust conductive framework and open three-dimensional porous structures. However, their salt adsorption capacities (SACs) are limited by the bland macropores and poor compatibility with aqueous environments. Herein, hierarchical porous nitrogen-doped spray-dried graphene (N-SDG) is prepared through a spray-drying method followed by low-temperature nitrogen doping. The resulting material exhibits hierarchical porosity and a nitrogen-rich carbon framework which demonstrates an improved SAC of 19.6 mg g^{-1} in 500 mg L^{-1} NaCl solution, amongst the highest reported for graphene-based CDI materials. The method herein demonstrates a commercially attractive approach for the production of N-doped porous graphene material for CDI applications. These findings are expected to underpin new developments in low-cost graphene-based materials for a range of applications.

1. Introduction

Capacitive deionization (CDI) has attracted increasing research attention as an energy-efficient and cost-effective technology for the desalination of brackish and saline water.^[1–3] Compared to conventional desalination methods such as reverse osmosis and distillation-based processes, CDI operates via the reversible electro-sorption of salt ions at the ultra-low voltage (1–2 V), low feed pressure and ambient temperature, making it appropriate for portable consumer devices through to large utility-scale installations. Recently, great efforts have centred on the design of high

performance electrode materials with enhanced salt adsorption capacities to boost CDI performance.^[4–6] Several classes of porous carbonaceous electrodes have been investigated including activated carbons (ACs),^[7,8] ordered mesoporous carbons (OMC),^[9–11] three-dimensional (3D) graphene foams,^[12–14] porous carbon spheres,^[15–17] hierarchically porous carbon monoliths^[18,19] and carbon fibers.^[20–23] Among these, 3D graphene foams have attracted particular attention due to their robust conductive framework and accessible 3D porosities.^[12–14,24] However, the CDI performances achieved by 3D structuring alone can only reach salt adsorption capacities (SACs) of 5.39 to 14.9 mg g^{-1} . In order to enhance CDI performances, in-plane nanopores have been generated in graphene


sheets by electrochemical activation^[25] and by hydrothermal treatment,^[12] but these techniques show only limited improvement, reaching SACs of 14.25 and 15.0 mg g^{-1} respectively. The limited CDI performances of 3D graphene foams are largely limited by their unsatisfactory wettability,^[14,24] as graphene and reduced graphene oxide surfaces are generally hydrophobic and in poor compatibility with aqueous environments.

Nitrogen doping^[13,26,27] and grafting of amino and sulfonic functional groups on graphene frameworks^[28] have also been applied to enhance the wettability and increase adsorption sites with corresponding boosts in CDI performance. However, these methods are primarily focused on the chemical modification of bland graphene foams and do not provide the hierarchical porosity required for high level salt uptake. Compositing graphene with porous carbon structures provides another strategy to introduce porosity and heteroatom functionality to the composites, while simultaneously preventing the restacking of graphene sheets.^[29–31] For example, graphene@microporous carbon composites with thin carbon layers were synthesized using graphene oxide sheets with conformal polyvinyl alcohol coatings.^[30] Although CDI performances surpassed traditional ACs, this method can only provide small micropores ($<2 \text{ nm}$) in the composite framework which limits the diffusion of salt to internal surface area and limits adsorption capacities. Furthermore, the complicated synthesis procedure requiring hydrothermal treatment, freeze drying, carbonization and activation of the composite material restricts their scalable production for practical applications. Recently, ultrathin nitrogen doped carbon coated graphene has been prepared by growing a metal organic

O. Noonan, Y. Kong, Y. Liu, M. Kalantari, A. Kumar Nanjundan, X. Huang, C. Yu

Australian Institute for Bioengineering and Nanotechnology
The University of Queensland
Brisbane, QLD 4072, Australia
E-mail: c.yu@uq.edu.au

C. Yu
School of Chemistry and Molecular Engineering
East China Normal University
Shanghai 200241, P. R. China

 The ORCID identification number(s) for the author(s) of this article can be found under <https://doi.org/10.1002/aesr.202100190>.

© 2022 The Authors. Advanced Energy and Sustainability Research published by Wiley-VCH GmbH. This is an open access article under the terms of the Creative Commons Attribution License, which permits use, distribution and reproduction in any medium, provided the original work is properly cited.

DOI: 10.1002/aesr.202100190

framework layer on graphene oxide nanosheets.^[31] After carbonization, the sandwich-like structures exhibited high surface areas, good electrical conductivity and uniform nitrogen doping. However only microporous structuring was obtained, which limited SAC to 17.5 mg g^{-1} . Importantly, the aforementioned approaches rely on graphene oxides synthesized through variations of the Hummer method,^[32] which is cost-prohibitive and impractical for large scale processing. It remains a significant challenge to prepare low-cost porous graphene with adequate hierarchical porous structures and nitrogen doping to provide competitive CDI performances.

In this work, we prepared nitrogen-doped graphene with the hierarchical porous structure through a low-cost spray drying and soft-nitriding strategy. The synthesized materials exhibited 3D hierarchical porosities including $\approx 3 \text{ nm}$ mesopores and abundant macropores with a high nitrogen content of 6.3 at%. The hierarchical porosity, conductive framework and enhanced wettability from nitrogen doping resulted in an improved SAC of 19.6 mg g^{-1} compared to control materials prepared without nitrogen doping (14.3 mg g^{-1}) or hierarchical porous structuring (5.75 mg g^{-1}). This work demonstrates a cost-effective method with scalable production potential for the preparation of graphene materials for high-performance CDI and paves the way for the further development of high-property graphene-based materials for various applications.

2. Results and Discussion

Spray dried graphene (SDG) was prepared via the spray pyrolysis of an aqueous suspension of electrochemically exfoliated graphene (EEG) mixed with commercial grade block copolymer surfactant (Pluronic F127). After carbonization of the EEG/surfactant composite, porous SDG materials composed of crumpled graphene nanosheets were produced. The as-prepared SDG was further annealed with urea at 350°C under nitrogen flow to yield nitrogen-doped spray dried graphene (N-SDG). Scanning electron microscopy (SEM) images of SDG and N-SDG materials (Figure 1a,b) reveal the macroporous morphology and the crumpled graphene pore walls. Measured from high magnification SEM images shown in Figure 1c,d, the size of graphene nanosheets is around several micrometers. Transition electron microscopy (TEM) characterizations indicate the presence of thin folded nanosheets, confirming the crumpled material topology for both samples (Figure 1e,f). Some areas of uneven contrast indicate the presence of a thin patchy surface on the N-SDG sheets. This is not visible in TEM images of pristine EEG annealed without surfactant assisted spray drying (Figure S1, Supporting Information), indicating that the patchy surfaces result from the thermal perforation during surfactant pyrolysis.^[33]

Further structural information is obtained by nitrogen adsorption analysis (Figure 2). Nitrogen adsorption isotherms (Figure 2a) show a majority of nitrogen uptake at high relative pressures for N-SDG and SDG, indicating the presence of abundant macropores in the two materials. The specific surface areas of N-SDG ($74.7 \text{ m}^2 \text{ g}^{-1}$) and SDG ($141 \text{ m}^2 \text{ g}^{-1}$) are significantly lower than the theoretical surface area of monolayer graphene ($\approx 2630 \text{ m}^2 \text{ g}^{-1}$), suggesting the spray dried materials are

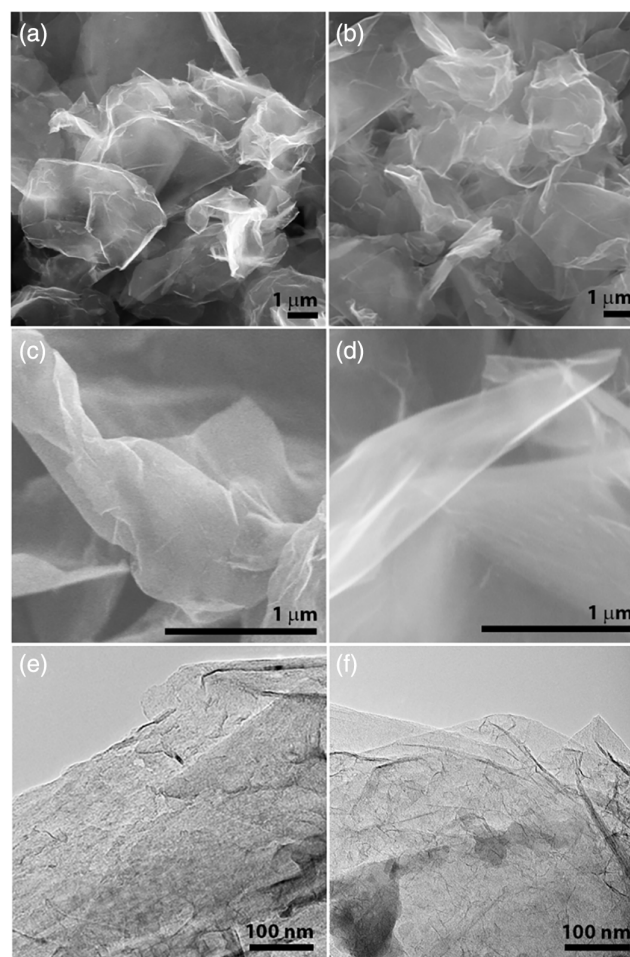


Figure 1. a–d) SEM images and e,f) TEM images of N-SDG (a,c,e) and SDG (b,d,f).

composed of few-layer graphene platelets rather than monolayers. The reduction in surface area observed for N-SDG suggests nitrogen-rich carbons with low surface area may have formed at the surface of graphene platelets during soft-nitriding. In contrast, pristine EEG prepared without spray drying exhibits a surface area of $16.8 \text{ m}^2 \text{ g}^{-1}$, which indicates the spray drying step is crucial for preventing excessive restacking of graphene sheets. Pore size distribution curves exhibit distinctive peaks at the pore diameter of around 100 nm for both N-SDG and SDG (Figure 2b, Table 1), which can be ascribed to the pore voids formed by the assembly of crumpled graphene sheets during spray drying. Pore size distributions centered around 3 nm are also detected for N-SDG and SDG, which arise from the surface nanopores generated by thermal perforation.^[33] In contrast, no obvious porosity can be detected for EEG, suggesting the spray drying process is critical for meso and macropore formation.

The composition of SDG materials is elucidated by X-ray photoelectron spectroscopy (XPS) (Figure 3a). The general survey results of N-SDG identify carbon, nitrogen and oxygen in the surface region with a nitrogen atom abundance of 6.3 at%.

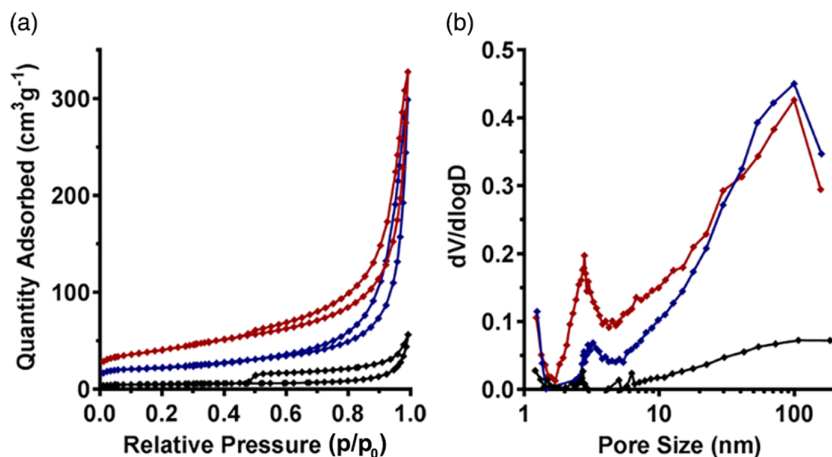


Figure 2. a) Nitrogen adsorption isotherms and b) pore size distributions from adsorption branch for N-SDG (blue), SDG (red) and EEG (black).

Table 1. Physical characteristics and salt adsorption capacities.

	S_{BET} [$\text{m}^2 \text{g}^{-1}$]	V_{PORE} [$\text{cm}^3 \text{g}^{-1}$]	$D_{\text{BJH ads.}}$ [nm]	$I_{\text{D}}/I_{\text{G}}$	N content [at%]	SAC [mg g^{-1}]
N-SDG	74.7	0.47	3.2, 100	1.00	6.30	19.6
SDG	141	0.51	2.7, 100	0.67	0.00	14.3
EEG	16.8	0.08	100	0.46	0.00	5.75

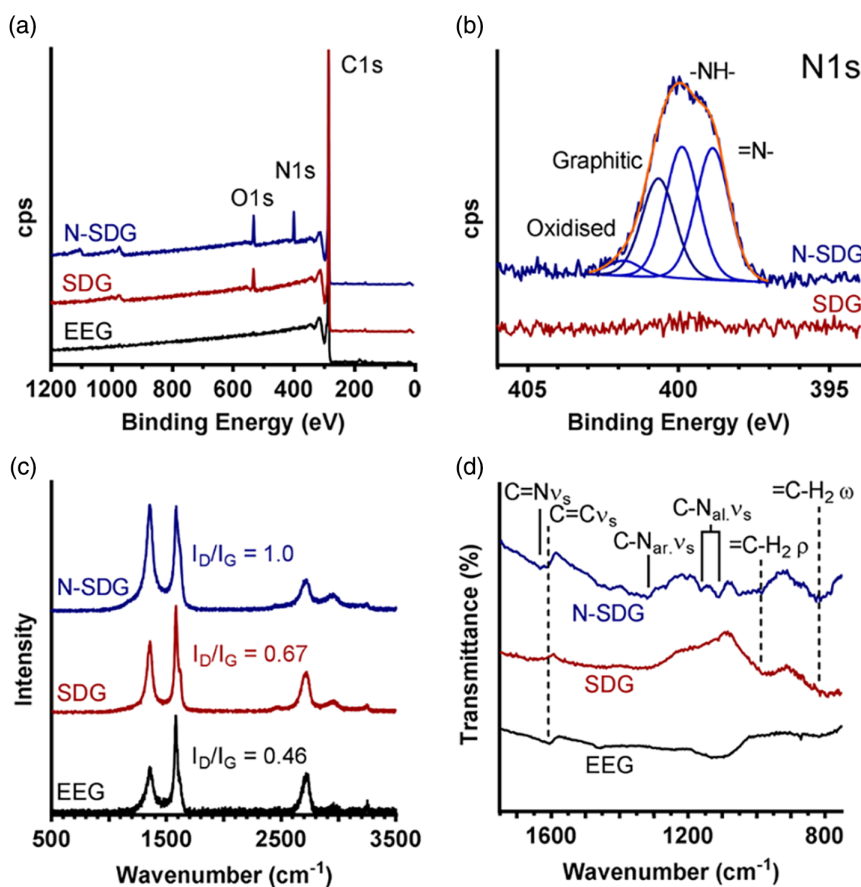


Figure 3. a) XPS wide scan and b) high resolution N1s scans, c) Raman spectra and d) FTIR spectra for N-SDG (blue), SDG (red) and EEG (black).

SDG exhibits carbon and oxygen peaks only, which confirms nitrogen doping in N-SDG originates from the soft nitriding process. EEG on the other hand shows a strong graphitic carbon peak with negligible nitrogen and oxygen, indicating extra oxygen is introduced during the spray drying and pyrolysis steps. High resolution scans of the N1s peak for N-SDG (Figure 3b) are deconvoluted into four distinct peaks with full width at half maximum values of 1.3 ± 0.001 eV. These peaks can be assigned to the known nitrogen bonding environments of pyridinic (398.9 eV), pyrrolic (399.9 eV), graphitic (400.7 eV) and oxidized nitrogen (401.8 eV) and display relative abundances of 35%, 35%, 26% and 4%, respectively. This fitting is consistent with expectations for nitrogen doped carbon produced by a similar soft-nitriding method.^[34] Pyridinic-N and pyrrolic-N are often considered as electrochemically active sites for the fast charge transfer, while graphitic-N is beneficial for the electrical conductivity of carbon frames.^[35] Collectively, these N species would contribute to the improved CDI performance.

Reductions in the degree of graphitic ordering of N-SDG materials after carbonization and soft-nitriding are detected using Raman spectroscopy (Figure 3c). The spectra for N-SDG, SDG and EEG all exhibit sharp adsorption bands at 1355 and 1587 cm^{-1} which correspond to the disordered (D) and ordered graphitic (G) vibrational modes of graphitic materials, respectively.^[36] Comparing the relative intensities of D and G bands (I_D/I_G) provides a convenient indicator of the graphitization degree of the carbon material. This value increases from 0.46 through 0.67 to 1.00 for the EEG, SDG and N-SDG respectively, indicating a larger amount of disordered carbon is present in N-SDG and SDG as compared with EEG. This can be ascribed to the increase in non-graphitized carbon content arising from perforated graphene in spray-dried materials. The increase of I_D/I_G from SDG to N-SDG indicates that additional disordered carbon components are induced after soft-nitriding.

Details on the functional groups conferred to the SDG materials during soft-nitriding are investigated by Fourier transform infrared (FT-IR) spectroscopy (Figure 3d). Several new absorptions for N-SDG appearing at 1635 , 1320 , 1164 and 1110 cm^{-1} which are absent in the EEG and SDG spectra can be ascribed to aromatic C=N, aromatic C-N and two aliphatic C-N stretch vibrations, respectively,^[37,38] confirming results from XPS that nitrogen is present both in in-ring and amorphous carbon environments. The band at 1605 cm^{-1} corresponds to in-ring C=C resonances is visible in the annealed EEG, SDG and N-SDG materials and can be ascribed to vibrations in the graphene scaffold. Absorptions detected at 990 and 820 cm^{-1} however are only observed for SDG and N-SDG and can be assigned to in-plane and out-of-plane alkene =C-H bending, respectively. Together with information from XPS and Raman spectroscopy, these results suggest additional nitrogen rich carbon has been deposited after spray drying and soft-nitriding. These findings are consistent with nitrogen doped carbon deposition via urea-mediated soft-nitriding.^[34] Under mild pyrolysis conditions, urea undergoes decomposition into isocyanic acid and ammonia groups which can then react with oxygen containing moieties on the surface of carbon and initiate deposition of a nitrogen rich amorphous carbon layer on the surface of SDG materials.

CDI performance of SDG materials (Figure 4a) is evaluated using a lab made flow through CDI device.^[29] SAC for N-SDG reaches an impressive value of 19.6 mg g^{-1} (7.84 wt% desalination rate) in 500 mg L^{-1} NaCl at 1.4 V. This represents a clear improvement from the value obtained by SDG under identical conditions (14.3 mg g^{-1} , 5.72 wt%) and pristine EEG (5.75 mg g^{-1} , 2.30 wt%), indicating nitrogen modification by soft-nitriding plays a crucial role in improving SAC. This may be attributed to the enhanced wettability resulting from the nitrogen functionality in N-SDG. It is noteworthy that SAC increases despite the reduction in BET surface area, suggesting the effect of wettability rather than surface area is dominant. The electric conductivity variations of NaCl solutions also show that N-SDG could quickly bring down the solution conductivity during the CDI tests (Figure S2, Supporting Information). The corresponding CDI Ragone plots (i.e., salt adsorption rate (SAR) vs SAC) are shown in Figure S3, Supporting Information, further suggesting that N-SDG more effectively performs desalination at a greater rate than either SDG or EEG. The initial current response and corresponding charge efficiencies (Figure 4b) for the two samples indicates N-SDG achieves higher charge utilization over the same time period, which may arise from a decrease in co-ion expulsion for N-SDG facilitated by nitrogen induced charge irregularities on the material surface. Cycling performance of the N-SDG electrodes (Figure 4c) reveals highly reversible salt uptake with near 100% retention of SAC between cycles confirming the suitability of N-SDG for continuous CDI application. The CDI performances of N-SDG including SAC and cycling stability are amongst the highest reported for graphene-based CDI materials (Table S1, Supporting Information).

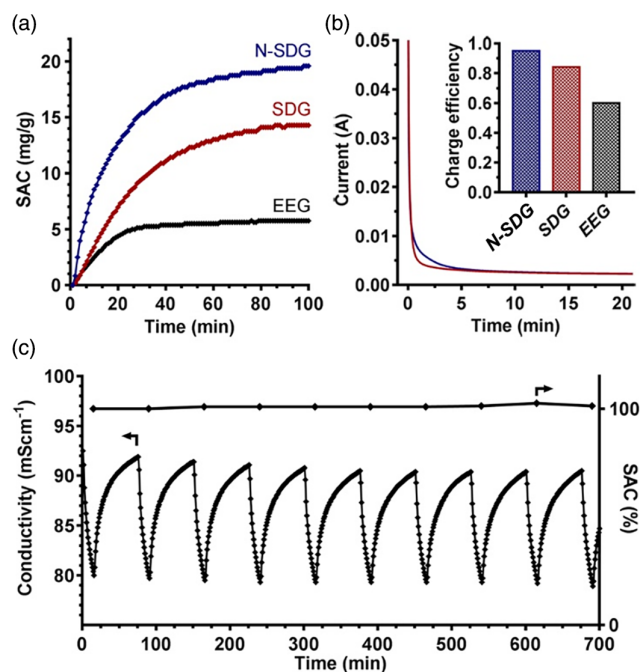


Figure 4. a) Salt adsorption capacity and b) initial current response for SDG materials at 500 mg L^{-1} NaCl at 1.4 V. Inset in (b) shows charge efficiency at 20 min. c) Electrodesorption cycling (left axis) and capacity retention (right axis) for SDG-N cycled between 1.4 and 0 V in 500 mg L^{-1} NaCl.

The role of nitrogen functionality for improved salt electro-sorption in SDG materials is further examined using cyclic voltammetry (CV) and galvanic charge (GC) cycles in 0.5 M NaCl. CV scans of N-SDG at increasing rates from 40 to 150 mV s^{-1} reveal quasi-rectangular profiles with good symmetry (Figure 5a) indicating charge storage is predominantly capacitive with negligible faradaic side reactions. Comparison of the CV profiles for N-SDG and SDG at 100 mV s^{-1} (Figure 5b) reveal an enlargement of integrated area for N-SDG indicating the enhanced EDL formation for this material. GC cycling for N-SDG and SDG exhibit near symmetrical triangular profiles at 2 A g^{-1} (Figure 5c) confirming the good reversibility of the capacitive charge storage process. The increase in specific capacitance observed for N-SDG compared to SDG over current densities ranging from 2 to 20 A g^{-1} (Figure 5d) confirms the importance of nitrogen functionality for enhancing charge immobilization on the CDI electrodes.

The manufacturing costs of N-SDG materials at the lab scale was estimated to be $\$27.8 \text{ kg}^{-1}$, based on bulk pricing of commercially available precursors and approximate processing costs (Table S2, Supporting Information).^[39] This value is far lower than estimates for other graphene-based materials prepared by conventional methods. For example, the price of commercially available chemically exfoliated GO and rGO in 2022 was $\approx \$46\,300 \text{ USD kg}^{-1}$ (Graphenea Inc., Massachusetts USA). Lowering the production costs of high performance graphene-based CDI materials is expected to promote the commercial uptake of these materials and increase the accessibility of CDI technologies globally.

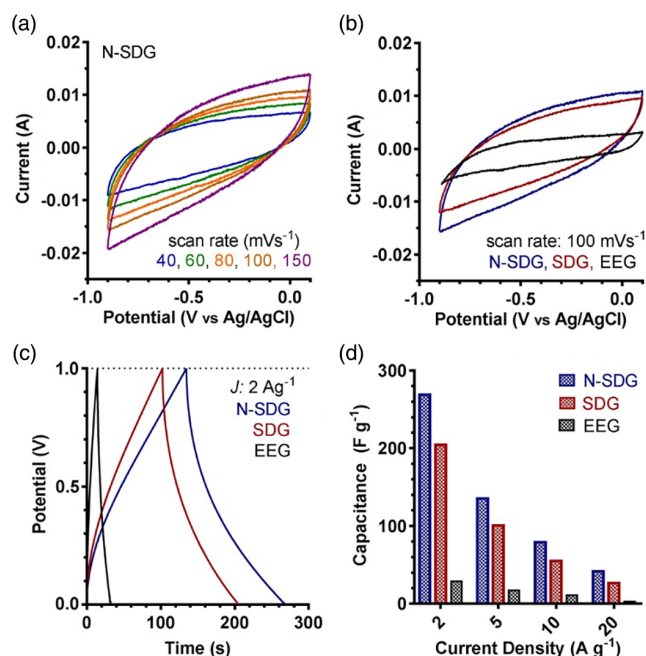


Figure 5. Cyclic voltammetry of a) N-SDG at various scan rates and b) N-SDG (blue) compared with SDG (red) at 100 mV s^{-1} . c) Galvanic cycling for N-SDG (blue) and SDG (red) at 2 A g^{-1} and d) specific capacitance values obtained at increasing current densities in 0.5 M NaCl electrolyte.

3. Conclusion

In summary, nitrogen-doped hierarchical porous graphene has been prepared via a spray drying and low-temperature nitrogen doping process. The resulting material exhibited high salt adsorption capacity (19.6 mg g^{-1} at 500 mg L^{-1} and 1.4 V) and excellent cycling stability, compared to control materials prepared without nitrogen doping (14.3 mg g^{-1}). The enhanced performance was ascribed to the improved electrode wettability and electronic conductivity resulting from the abundant nitrogen content (6.3 at%). The low cost, wide availability and low toxicity of material precursors along with simple and well-established processing methods provides a commercially attractive route to the scalable manufacturing of high performance CDI electrode materials. These findings are expected to underpin new developments in the low-cost processing of graphene-based advanced materials for various applications.

4. Experimental Section

Electrochemical Exfoliation of Graphene: Electrochemically exfoliated graphene (EEG) was prepared by modification of a previously reported method.^[40] Briefly, graphite foil (Alfa Aesar, 99.9%, 1 g) was immersed in a bath of Na_2SO_4 (0.1 M, 1 L). An anodic potential of 10 V was applied to the graphite foil by employing a stainless steel counter electrode immersed at a spacing of ≈ 1 cm. The sediment was collected and rinsed by 5 centrifugation/redispersion cycles in pure water followed by rising in isopropanol. The electrochemically expanded graphite flakes were further subjected to ultrasonic exfoliation in isopropanol for 30 min leaving a stable suspension of few layer EEG. Centrifugation of this suspension yielded EEG sediment which was used directly.

Spray Dried Graphene and Soft-Nitriding: Spray dried graphene was prepared by dispersing EEG (1 g) in deionized water (200 mL) containing Pluronic F127 (Sigma, 6 mg mL^{-1}) and sonicating for 3 h to obtain a homogenous mixture. The mixture was then processed in a spray drier (Buchi mini spray drier – B290) with an inlet temperature of 220 $^{\circ}\text{C}$, aspirator rate of 100%, atomizer pressure of 60 psi and a pump rate of 3 mL min^{-1} . The as synthesized sample was collected in a cyclonic separator and carbonized under nitrogen flow at 400 $^{\circ}\text{C}$ for 3 h under heating and cooling rates of 2 $^{\circ}\text{C min}^{-1}$. The as-prepared SDG (1 g) was further annealed with urea (2 g) at 350 $^{\circ}\text{C}$ under nitrogen flow to yield nitrogen-doped spray dried graphene (N-SDG).

Electrochemical Characterization: Working electrodes consisted of active material, acetylene black, and polytetrafluoroethylene (PTFE) mixed in an 80:10:10 wt% ratio and pressed onto graphite foil current collectors. The weight of active material per electrode was approximately 1 mg occupying an area of 1 cm^2 . Electrochemical tests including cyclic voltammetry (CV) and galvanostatic charge/discharge (GC) and Electrochemical impedance spectroscopy (EIS) tests were performed on a Solartron Multistat electrochemical workstation using a three-electrode cell setup in 0.5 M NaCl electrolyte with platinum wire and Ag/AgCl (0.5 M KCl) electrodes as counter and reference electrodes, respectively.

CDI Performance: A lab made flow-by CDI apparatus was constructed for application testing. Apparatus details can be found in supporting information. Identical CDI electrodes were fabricated by mixing active material, acetylene black and PTFE in an 80:10:10 wt% ratio. The mixture containing 50 mg active material was doctor bladed onto graphite foil current collectors to cover an area of 50 \times 100 mm. Saline water (25 mL) was continuously recirculated through the CDI cell using a peristaltic pump. The solution flow rate was 25 mL min^{-1} . Ionic conductivity measurements were obtained using a Horriba Laqua F-70 conductivity meter. A Solartron Multistat electrochemical workstation was used to the control voltage and record current flow supplied to the cell.

SAC is calculated according to Equation (1)

$$\text{SAC} = \frac{(C_u - C_v)V}{m} \quad (1)$$

Where C_u is the initial concentration (mg L^{-1}), C_v is the final concentration at time t (mg L^{-1}), V is the volume of NaCl solution (L) and m is the active mass of the electrodes (g).

Charge efficiency (Λ) is calculated according to Equation (2)

$$\Lambda = \frac{\Gamma \times F}{\Sigma} \quad (2)$$

Where Γ is the molar salt adsorption capacity (mol g^{-1}), F is faradays constant (96485 C mol^{-1}), Σ is the total charge transferred between the electrodes (C g^{-1}).

Supporting Information

Supporting Information is available from the Wiley Online Library or from the author.

Acknowledgements

We acknowledge the financial support from Australian Research Council, Queensland Government, China Scholarship Council and the University of Queensland. We also thank Australian National Fabrication Facility, Australian Microscopy and Microanalysis Research Facility at the Centre for Microscopy and Microanalysis, the University of Queensland for technical assistance.

Conflict of Interest

The authors declare no conflict of interest.

Data Availability Statement

The data that support the findings of this study are available from the corresponding author upon reasonable request.

Keywords

capacitive deionization, graphene, nitrogen doping, porous material, spray drying

Received: November 28, 2021

Revised: January 12, 2022

Published online: February 5, 2022

- [1] F. A. Al Marzooqi, A. A. Al Ghaferi, I. Saadat, N. Hilal, *Desalination* **2014**, 342, 3.
- [2] S. Porada, R. Zhao, A. van der Wal, V. Presser, P. M. Biesheuvel, *Prog. Mater. Sci.* **2013**, 58, 1388.
- [3] M. E. Suss, S. Porada, X. Sun, P. M. Biesheuvel, J. Yoon, V. Presser, *Energy Environ. Sci.* **2015**, 8, 2296.
- [4] Z.-H. Huang, Z. Yang, F. Kang, M. Inagaki, *J. Mater. Chem. A* **2017**, 5, 470.
- [5] P. Liu, T. Yan, L. Shi, H. S. Park, X. Chen, Z. Zhao, D. Zhang, *J. Mater. Chem. A* **2017**, 5, 13907.
- [6] Y. Liu, C. Nie, X. Liu, X. Xu, Z. Sun, L. Pan, *RSC Adv.* **2015**, 5, 15205.
- [7] J. W. Blair, G. W. Murphy, *Saline Water Conversion* **1960**, 20, 206.
- [8] G. W. Murphy, J. L. Cooper, S. United, *Activated Carbon Used as Electrodes in Electrochemical Demineralization of Saline Water*, U.S. Department of the Interior, Washington, DC **1969**.
- [9] Z. Peng, D. Zhang, L. Shi, T. Yan, *J. Mater. Chem.* **2012**, 22, 6603.
- [10] a) C. Tsouris, R. Mayes, J. Kiggans, K. Sharma, S. Yiacoymi, D. De Paoli, *Environ. Sci. Technol.* **2011**, 45, 10243; b) Q. Li, X. T. Xu, J. R. Guo, J. P. Hill, H. S. Xu, L. X. Xiang, C. Li, Y. Yamauchi, Y. Y. Mai, *Angew. Chem. Int. Ed.* **2021**, 60, 26528.
- [11] L. Zou, L. Li, H. Song, G. Morris, *Water Res.* **2008**, 42, 2340.
- [12] W. Shi, H. Li, X. Cao, Z. Y. Leong, J. Zhang, T. Chen, H. Zhang, H. Y. Yang, *Sci. Rep.* **2016**, 6, 18966.
- [13] X. Xu, Z. Sun, D. H. C. Chua, L. Pan, *Sci. Rep.* **2015**, 5, 11225.
- [14] X. Xu, L. Pan, Y. Liu, T. Lu, Z. Sun, D. H. C. Chua, *Sci. Rep.* **2015**, 5, 8458.
- [15] X. Xu, H. Tang, M. Wang, Y. Liu, Y. Li, T. Lu, L. Pan, *J. Mater. Chem. A* **2016**, 4, 16094-16100.
- [16] Y. Li, J. Qi, J. Li, J. Shen, Y. Liu, X. Sun, J. Shen, W. Han, L. Wang, *ACS Sustain. Chem. Eng.* **2017**, 5, 6635-6644.
- [17] H. Wang, L. Shi, T. Yan, J. Zhang, Q. Zhong, D. Zhang, *J. Mater. Chem. A* **2014**, 2, 4739-4750.
- [18] Y. Li, I. Hussain, J. Qi, C. Liu, J. Li, J. Shen, X. Sun, W. Han, L. Wang, *Sep. Purif. Technol.* **2016**, 165, 190-198.
- [19] X. Wen, D. Zhang, T. Yan, J. Zhang, L. Shi, *J. Mater. Chem. A* **2013**, 1, 12334.
- [20] a) R. L. Zornitta, F. J. García-Mateos, J. J. Lado, J. Rodríguez-Mirasol, T. Cordero, P. Hammer, L. A. M. Ruotolo, *Carbon* **2017**, 123, 318-333; b) Z. B. Ding, X. T. Xu, J. B. Li, Y. Q. Li, K. Wang, T. Lu, Md. S. A. Hossain, M. A. Amin, S. H. Zhang, L. K. Pan, Y. Yamauchi, *Chem. Eng. J.* **2022**, 430, 133161; c) X. T. Xu, J. Tang, Y. V. Kaneti, H. B. Tan, T. Chen, L. K. Pan, T. Yang, Y. Bando, Y. Yamauchi, *Mater. Horiz.* **2020**, 7, 1404.
- [21] C. Kim, P. Srimuk, J. Lee, S. Fleischmann, M. Aslan, V. Presser, *Carbon* **2017**, 122, 329.
- [22] G.-X. Li, P.-X. Hou, S.-Y. Zhao, C. Liu, H.-M. Cheng, *Carbon* **2016**, 101, 1.
- [23] G. Wang, C. Pan, L. Wang, Q. Dong, C. Yu, Z. Zhao, J. S. Qiu, *Electrochim. Acta* **2012**, 69, 65.
- [24] H. Wang, D. Zhang, T. Yan, X. Wen, J. Zhang, L. Shi, Q. Zhong, *J. Mater. Chem. A* **2013**, 1, 11778.
- [25] M. S. Zoromba, M. H. Abdel-Aziz, M. Bassyouni, S. Gutub, D. Demko, A. Abdelkader, *ACS Sustain. Chem. Eng.* **2017**, 5, 4573.
- [26] X. Xu, L. Pan, Y. Liu, T. Lu, Z. Sun, *J. Colloid Interface Sci.* **2015**, 445, 143.
- [27] A. M. Abdelkader, D. J. Fray, *Nanoscale* **2017**, 9, 14548.
- [28] P. Liu, H. Wang, T. Yan, J. Zhang, L. Shi, D. Zhang, *J. Mater. Chem. A* **2016**, 4, 5303.
- [29] O. Noonan, Y. Liu, X. D. Huang, C. Z. Yu, *J. Mater. Chem. A* **2018**, 6, 14272.
- [30] Z. Y. Leong, G. Lu, H. Y. Yang, *Desalination* **2019**, 451, 172.
- [31] a) M. Wang, X. T. Xu, J. Tang, S. J. Hou, M. S. A. Hossain, L. K. Pan, Y. Yamauchi, *Chem. Commun.* **2017**, 53, 10784; b) J. R. Guo, X. T. Xu, J. P. Hill, L. P. Wang, J. J. Dang, Y. Q. Kang, Y. L. Li, W. S. Guan, Y. Yamauchi, *Chem. Sci.* **2021**, 12, 10334.
- [32] W. S. Hummers, R. E. Offeman, *J. Am. Chem. Soc.* **1958**, 80, 1339.
- [33] Y. Q. Kong, C. Tang, X. D. Huang, A. K. Nanjundan, J. Zou, A. J. Du, C. Z. Yu, *Adv. Funct. Mater.* **2021**, 31, 2010569.
- [34] B. Liu, H. Yao, W. Song, L. Jin, I. M. Mosa, J. F. Rusling, S. L. Suib, J. He, *J. Am. Chem. Soc.* **2016**, 138, 4718-21.
- [35] a) J. Hou, C. Cao, F. Idrees, X. Ma, *ACS Nano* **2015**, 9, 2556; b) L. Sun, C. Tian, Y. Fu, Y. Yang, J. Yin, L. Wang, H. Fu, *Chem. Eur. J.* **2014**, 20, 564; c) L. Lai, J. R. Potts, D. Zhan, L. Wang, C. K. Poh, C. Tang, H. Gong, Z. Shen, J. Lin, R. S. Ruoff, *Energy Environ. Sci.* **2012**, 5, 7936.
- [36] Z. Zafar, Z. H. Ni, X. Wu, Z. X. Shi, H. Y. Nan, J. Bai, L. T. Sun, *Carbon* **2013**, 61, 57.

- [37] N. A. Kumar, H. Nolan, N. McEvoy, E. Rezvani, R. L. Doyle, M. E. G. Lyons, G. S. Duesberg, *J. Mater. Chem. A* **2013**, *1*, 4431.
- [38] A. Amiri, G. Ahmadi, M. Shanbedi, M. Savari, S. N. Kazi, B. T. Chew, *Sci. Rep.* **2015**, *5*, 17503.
- [39] V. H. Holsinger, A. J. McAloon, C. I. Onwulata, P. W. Smith, *J. Dairy Sci.* **2000**, *83*, 2361.
- [40] K. Parvez, Z.-S. Wu, R. Li, X. Liu, R. Graf, X. Feng, K. Müllen, *J. Am. Chem. Soc.* **2014**, *136*, 6083.